ELSEVIER

3D knitted energy storage textiles using MXene-coated yarns

Ariana Levitt [1,2], Dylan Hegh [3], Patrick Phillips [3], Simge Uzun [1,2], Mark Anayee [1], Joselito M. Razal [3], Yury Gogotsi [1,*], Genevieve Dion [2,*]

[1] A.J. Drexel Nanomaterials Institute and Department of Materials Science and Engineering, Drexel University, 3141 Chestnut St., Philadelphia, PA 19104, United States
[2] Center for Functional Fabrics, Drexel University, 3141 Chestnut St., Philadelphia, PA 19104, United States
[3] Institute for Frontier Materials, Deakin University, Geelong, VIC 3216, Australia

Textile-based energy storage devices offer an exciting replacement for bulky and uncomfortable batteries in commercial smart garments. Fiber and yarn-based supercapacitors, currently dominating research in this field, have demonstrated excellent performance below ~4 cm in length, but suffer at longer lengths due to increased resistance. Herein, a new architecture of wearable energy storage devices, 3D knitted supercapacitors, is designed and prototyped with the intention of exploiting the architecture of a knit textile to improve the performance of long yarn electrodes. While Computer-Aided Design (CAD) knitting is a ubiquitous technology for producing textiles, knitted energy storage devices have been largely unexplored due to the need for meters of highly conductive yarn electrodes that meet the strenuous strength and flexibility requirements for CAD knitting. MXenes, a family of solution processable and conductive two-dimensional (2D) materials, have been realized as inks, slurries, pastes, and now dyes for the development of on-paper, on-plastic, and on-textile microsupercapacitor electrodes. In this work, $Ti_3C_2T_x$ MXene was adopted as an active material for coating meters of commercial natural and synthetic yarns, enabling the production of knitted planar microsupercapacitors. The impact on electrochemical performance of knit structure and geometry was systematically studied in an attempt to produce energy storing textiles with power and energy densities that can be used for practical applications. The resulting energy storing textiles demonstrate high capacitance, up to 707 mF cm^{-2} and 519 mF cm^{-2} at 2 mV s^{-1} in 1 M H_3PO_4 and PVA-H_3PO_4 gel electrolyte, respectively, and excellent cycling stability over 10,000 cycles. This work represents an important step towards the mass production of MXene-based conductive yarns and 3D knitted energy storage devices and demonstrates how knit structure plays a significant role on device performance.

Introduction

As technology becomes increasingly more mobile, the next step is to integrate devices and functionalities into wearable textiles for applications including sensing [1,2], actuation [3,4], and wireless communication [5,6]. Many of these devices require power, motivating researchers to develop energy storage devices that are seamlessly integrated into textiles. Wearable textiles are required to be relatively soft, comfortable, and flexible, and as such the components of wearable smart textiles, including their power source, should be as well.

* Corresponding authors.
E-mail addresses: Gogotsi, Y. (yg36@drexel.edu), Dion, G. (gd63@drexel.edu).

 https://doi.org/10.1016/j.mattod.2020.02.005

To meet these design and performance criteria, numerous textile supercapacitor architectures have been explored, including fiber- and yarn-based devices [7–9] and fabric-based devices [10–13]. The former include fiber/yarn electrodes that were coated with an electrolyte and twisted or plied with one another. The latter include fabrics coated with an active material and electrolyte and sandwiched together. Electrode yarns can also be stitched into pre-existing fabrics and coated with an electrolyte to form a fabric device [12]. While short segments of fiber and yarn devices (typically <4 cm) have demonstrated high capacitance and energy density [14], they often suffer from high resistance at longer lengths, leading to reduced electrochemical performance [15–17]. For this reason, knitted electrodes are a promising alternative architecture for textile energy storage devices because yarns are manipulated into interconnected loops, allowing charges to move through the path of least resistance, rather than following the geometric path of the yarn through the knit structure [18]. As such, this problem of resistance growing linearly with yarn length can be circumvented by using knitting as a manufacturing platform for textile supercapacitors. In Computer-Aided Design (CAD) knitting, fabrics are programmed using a visual coding language, which provides the user with control over each knitting needle and yarn pathway. This technology is ideal for designing tunable and dimensional structures with varying densities and topologies, which is critical for the fabrication of complex textile devices, such as textile supercapacitors.

To our knowledge, since the first demonstration in 2014 of knitting activated carbon-based yarn electrodes on an industrial-scale machine [19], little effort has been made towards understanding and optimizing the electrochemical behavior of knitted energy storage devices. This can be attributed to two main challenges associated with the fabrication of textile supercapacitors. The first challenge relates to scaling the production of fiber and yarn electrodes [19,20], including both the synthesis of the selected active material and the conductive fiber/yarn fabrication method. For example, many works have been published on poly(3,4-ethylenedioxythiophene) (PEDOT)-based fiber and yarn supercapacitors, where PEDOT is deposited onto fiber surfaces using vapor-phase reactions or potentiostatic methods [21,22]. While these methods can be simple and cost-effective on a lab-scale, precise control required over environmental conditions, such as pressure and temperature, creates barriers for scaling. The second challenge, advanced manufacturing feasibility, relates to the mechanical properties of the fiber/yarn electrodes and the mechanical forces they will encounter during industrial textile manufacturing processes (knitting, weaving, etc.). During these processes, yarns are pulled through a series of tensioning devices, and in the case of knitting, dragged across beds of needles at speeds ranging from 0.03 m s^{-1} to 0.6 m s^{-1}, and bent into small loops with bending radii in the range of 0.5 to 2 mm (based on the needle gauge). As such, industrial textile fabrication can lead to damage or even breakage of the fiber/yarn during textile production. In sum, in order to incorporate fiber and yarn electrodes into textiles on a large scale, these materials must meet the strength and flexibility requirements of industrial textile production.

A promising new material for the development of large-scale yarn electrodes is $Ti_3C_2T_x$ (T_x represents surface terminations) MXene, a two-dimensional (2D) transition metal carbide that was discovered in 2011 [23]. $Ti_3C_2T_x$ is hydrophilic [24], allowing easy processing in water, and it exhibits superior electronic conductivity (10,000 S cm^{-1} as a thin film) compared to other solution processable nanomaterials [25]. In addition, due to its unique transition metal oxide-like surface, $Ti_3C_2T_x$ is capable of undergoing redox reactions at high charge–discharge rates, enabling high capacitance in acidic electrolytes [26,27]. Variation in sonication conditions and centrifugation during production allows precise control over the size of MXene flakes [28]. Control over flakes size is critical for fiber development, particularly for coating fibers of various diameters [14,29], and processing microfibers *via* wet spinning [30] and nanofibers *via* electrospinning [31]. Recent reports have demonstrated the outstanding electrochemical performance of $Ti_3C_2T_x$-based fibers [7,14,30,32], including wet-spun PEDOT/$Ti_3C_2T_x$ fibers [33], biscrolled $Ti_3C_2T_x$ fibers [7], and $Ti_3C_2T_x$-coated cellulose-based yarns [34]. We showed that cotton yarns loaded with up to 79 wt.% $Ti_3C_2T_x$ exhibited high conductivity (up to 200 S cm^{-1}) and length-specific capacitance (up to 760 mF cm^{-1} at 2 mV s^{-1} in 1 M H_2SO_4) and demonstrated their knittability [34]. More recently, we have etched large batches of Ti_3AlC_2 (up to 50 g) [35]; a promising step towards enabling large-scale coating of yarns with this material.

In this work, we demonstrate a method for the production of tens of meters of $Ti_3C_2T_x$-coated yarn electrodes and study how varying knit structure and geometry enables the tunable performance of knitted supercapacitors. To produce these yarn electrodes, cotton yarn (1-ply and 2 ply) and multifilament nylon fibers were coated with $Ti_3C_2T_x$ (referred to as MXene) using a yarn-coating platform. This work demonstrates the feasibility of automating the production of MXene-coated yarns, which could be replicated using existing coating processes in the textile industry. After coating, the yarns were knitted into textile energy storage devices using a commercial Shima Seiki 3D knitting machine. These devices were knitted in one piece; the electrodes were knitted on either side of an insulating yarn, as part of a small area on a larger textile. The impact on electrochemical performance of knit structure and geometry was investigated in an attempt to produce energy storing textiles with power and energy densities that can be used for practical applications. Finally, after the device design was selected, three devices were knitted in series to demonstrate a working prototype of a textile energy storage device. Using the processes employed in this work, automated yarn coating and industrial knitting technology, textile supercapacitors can be rapidly designed, programmed, prototyped, and ultimately, mass-produced. This is the first work in literature to study industrially relevant knitting parameters in designing textile-based supercapacitors from MXene yarns that can be continuously produced in fundamentally unlimited length scale.

Results and discussion

Automated yarn coating

Ten meters of cotton yarn and multifilament nylon fibers were coated with MXene using an automated yarn coating set-up to enable the development of knitted supercapacitors, as shown in Fig. 1. The optimization of this large-scale coating process was investigated based on previous work which employed a manual dip-coating process [34]. Metrics for successful scaling included the uniformity of the coating, the efficiency of the process (maximizing the uptake of MXene and minimizing waste), and the properties of the final yarn achieved (mass loading, resistance, and flexibility). As a reference, when coating manually, achieving a MXene loading of 0.3 mg cm^{-1} on 90 cm of 1-ply cotton yarn (150 T m^{-1}) using a 10–15 mg mL^{-1} MXene/water dispersion required approximately 12 dip cycles, equating to roughly 12 h of non-continuous labor. This arduous process further necessitated automation.

The coating process developed involved passing commercial yarns at a fixed rate through successive baths filled with MXene dispersions and collecting the dried, coated yarns onto a yarn winder (Fig. 1a). Several parameters, including the concentration and flake size of MXene solutions, the placement, length, and number of MXene baths on the coating line, the rate at which the yarns moved through the baths, and the drying time and mechanism, were carefully tuned to achieve the desired properties. First, MXene dispersions were prepared for yarn coating by dispersing delaminated $Ti_3C_2T_x$ flakes in deionized water at a concentration of 10–15 mg mL^{-1} and probe sonicating for 20 min. The concentration and conductivity of each batch of MXene was measured and calculated based on films produced from these solutions using vacuum-assisted filtration. The prepared films, shown in Fig. S1a and b, had conductivity values of 7676 ± 475 S cm^{-1} and 1681 ± 346 S cm^{-1} for as-synthesized and probe sonicated dispersions, respectively (Table S1). Although films made from smaller sonicated flakes had reduced conductivity compared with films made from larger as-synthesized flakes, small flakes were preferred for coating fibers/-yarns for knitting complex stitch patterns because they penetrated deeper into the yarn and better adhered to the fiber surface compared to large flakes. Large flakes created a shell around the yarn surface (Fig. S1c), which often cracked during bending around a fine knitting needle (Fig. S1d), potentially affecting the mechanical integrity of the yarns. Yarns coated with small flakes bent without noticeable cracking (Fig. S1e and f).

The flake size distribution and stacking order of $Ti_3C_2T_x$ was confirmed using dynamic light scattering (DLS) and X-ray diffraction (XRD), respectively. Briefly, DLS showed that 90–95% of flakes were approximately 150 nm in lateral size after probe sonication (Fig. S2a), compared with as-synthesized flakes, in which 83% of flakes were ~1 μm in lateral size. Scanning electron microscopy (SEM) images of representative as-synthesized and probe-sonicated flakes are shown in Fig. S2b. The XRD pattern of a film produced by vacuum-assisted filtration from a probe-sonicated MXene/water dispersion has a sharp (002) peak at $2\theta = 7.9°$, corresponding to an interlayer spacing of ~11.2 Å. The presence of additional (0 0 *l*) peaks confirmed the stacking order of MXene sheets along the c-axis (Fig. S2b) [36].

After preparation of the MXene dispersions, four baths made from vinyl tubing were placed along a commercial yarn coating line with 3 m between each bath. The baths were made from vinyl tubing to prevent MXene adhesion to the walls of the tube.

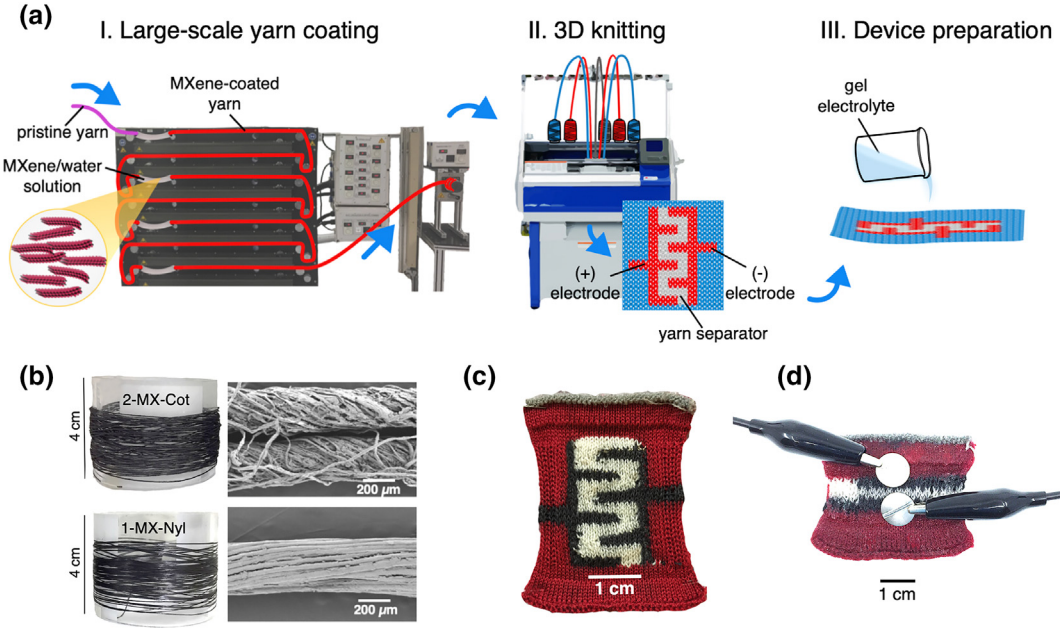

FIGURE 1

MXene-based textile energy storage device fabrication, from coated fibers to knitted textiles. (a) Schematic illustration of the large-scale production of MXene-coated yarns and 3D knitted energy storage devices, (b) optical images of ~10 meters of 2-ply MXene-coated cotton yarn (2-MX-Cot) and multifilament nylon fibers (1-MX-Nyl) and SEM images of the coated yarns, (c) image of a knitted textile with an interdigitated pattern made using MXene-coated cotton yarns (2-ply) as the electrodes, (d) image of an assembled knitted supercapacitor ready for electrochemical testing.

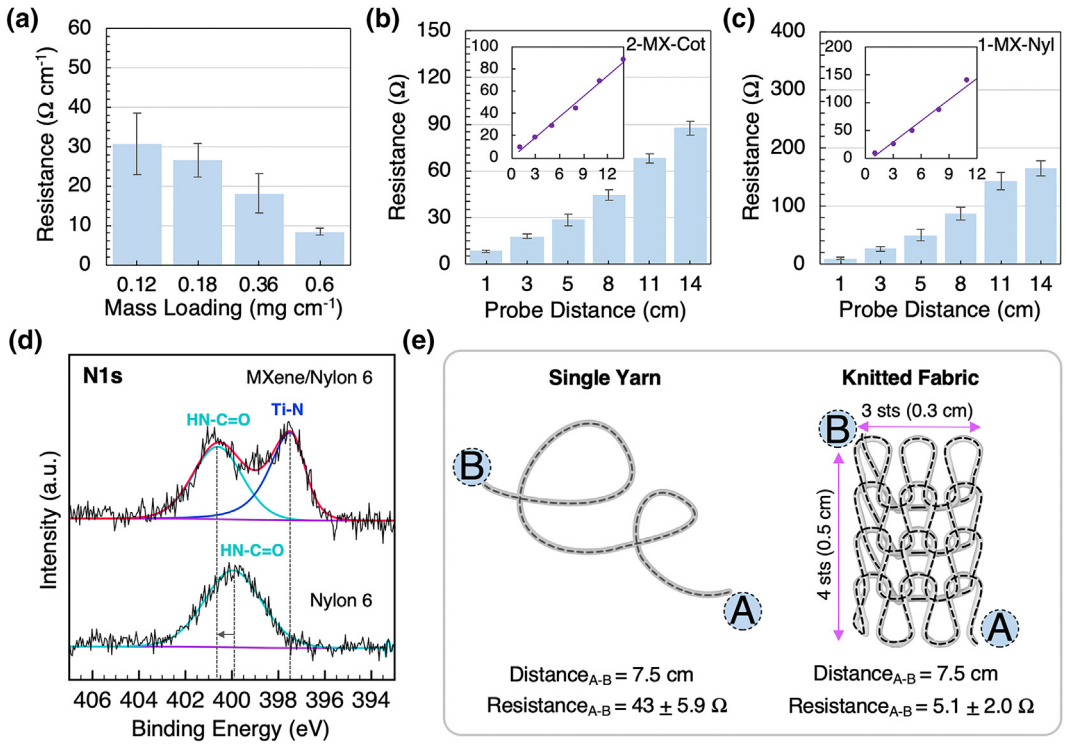

FIGURE 2

MXene-coated yarn properties (mass loading, resistance, and bonding). (a) resistance of 2-ply MXene-coated cotton yarns as a function of MXene loading, (b) resistance of 2-ply MXene-coated cotton (2-MX-Cot) yarns (0.6 mg cm^{-1} loading) as a function of yarn length, (c) resistance of MXene-coated nylon (1-MX-Nyl) fibers (0.22 mg cm^{-1} loading) as a function of yarn length, (d) XPS N1s core level spectra of pristine nylon fibers and MXene-coated nylon fibers, (e) end-to-end resistance of a 2-ply MXene-coated cotton yarn (0.6 mg cm^{-1} loading) (left) in comparison with the corner-to-corner resistance of a fabric knitted from the same yarn (sts = stitches).

They were spaced apart such that the yarns fully dried in air before entering the next bath, which was critical for restacking MXene flakes and increasing the MXene loading on the yarns. Each bath was filled with approximately 4 mL of MXene solution and the solutions were replenished throughout the coating process to ensure consistent residence time of the yarn in each bath. The yarns moved through the coating line at a speed of 0.4 m min^{-1}, providing a residence time of 18 s in each MXene bath and drying time of 9 min between baths. Yarns were collected onto a yarn winder and repeatedly fed through the coating line until the desired MXene loading was achieved. Ten meters of both cotton yarns and multifilament nylon fibers were coated, as shown in Fig. 1b. Throughout this work, MXene-coated yarns will be referred to by their number of plies and fiber substrate. For example, 1-MX-Nyl refers to 1-ply MXene-coated nylon fibers, 1-MX-Cot refers to 1-ply MXene-coated cotton yarns, and 2-MX-Cot refers to 2-ply MXene-coated cotton yarns.

SEM images of the pristine and coated fibers and yarns (Figs. 1b and S3) reveal that MXene flakes coat individual cotton and nylon fibers. For 2-MX-Cot, the MXene loading increased by 0.08–0.1 mg cm^{-1} with each coating cycle (i.e. pass through four baths). As shown in Fig. 2a, the resistance of the yarns decreased as a function of MXene mass loading, from 30.7 ± 7.8 Ω cm^{-1} at a loading of 0.12 mg cm^{-1} to 8.4 ± 0.9 Ω cm^{-1} at 0.6 mg cm^{-1} (~51 wt.%). The uptake rate of MXene onto nylon fibers was significantly slower; fibers achieved a loading of approximately 0.22 mg cm^{-1} with the same number of coating cycles. We speculate that the difference in MXene loading between the nylon fibers and cotton yarns is largely due to the surface area of the substrate. Increasing the number of nylon fibers in the bundle or using finer nylon fibers would likely increase the MXene loading. However, accounting for the mass of the pristine fibers, the MXene loading onto nylon fibers was only slightly less than onto 2-ply cotton yarns, 43 wt.% and 51 wt.%, respectively. For both 2-MX-Cot and 1-MX-Nyl, the resistance increased linearly with the length of the yarn, as shown in Fig. 2b and c, respectively. For example, the resistance increased from 8.40 Ω at 1 cm to 87.7 Ω at 14 cm for 2-MX-Cot (0.6 mg cm^{-1} loading, ~51 wt.%) and from 9.4 Ω to 164.2 Ω for 1-MX-Nyl (0.22 mg cm^{-1} loading, ~43 wt.%). These yarns, in addition to 1-MX-Cot with mass loading of 0.3 mg cm^{-1}, were selected for knitting devices because the resistance was sufficiently low (<10 Ω cm^{-1}) for use as supercapacitor electrodes, and the yarns maintained enough flexibility to bend around a 15-gauge knitting needle.

Prior to knitting, the adhesion between MXene and the fiber substrates was also considered. It was previously demonstrated that MXene adheres well to cotton fibers, as evident from a series of washing cycles, in which MXene-coated cotton fibers were exposed to elevated temperatures (up to 80 °C) under continuous stirring with minimal changes in resistance and mass [34]. To investigate the adhesion of MXene to nylon fibers, the interaction at the interface between MXene and nylon fibers was studied using X-ray photoelectron spectroscopy (XPS) (Figs. 2d, S4, and Table S2). In the N 1s spectrum (Fig. 2d), the pristine nylon

fibers exhibited one peak at ~399.9 eV [37], which was assigned to the NCO amide functional group. This peak was present in the MXene-coated fibers and shifted to higher binding energy (~400.7 eV), likely due to partial protonation of the amide group from –OH groups on the surface of MXene flakes [38,39]. A second peak appeared in the N 1s spectrum in the MXene-coated nylon fibers at ~397.5 eV, which was assigned to Ti-N bonding [40]. This peak was observed in other works involving $Ti_3C_2T_x$ and nitrogen-containing materials, such as (3-aminopropyl) triethoxysilane (APTES)-treated PET coated with MXene [29]. We speculate that this bond was formed through a dehydration reaction between an –OH group on the surface of MXene and a hydrogen atom from nylon's amide group, resulting in the release of water. These results indicate that there may be a covalent bond between $Ti_3C_2T_x$ MXene and nylon, suggesting good adhesion between nylon fibers and MXene flakes.

3D knitting of MXene-coated yarns

MXene-coated fibers and yarns were knitted into textile supercapacitors using a flat-bed industrial-scale weft knitting machine, illustrated in Fig. 1a. To demonstrate feasibility of knitting textile electrodes, MXene-coated yarns were knitted into 0.3 cm × 0.5 cm fabrics using 7.5 cm of yarn. The resistance measured diagonally across a knitted fabric of 2-ply MXene-coated cotton yarns, as illustrated in Fig. 2e, was 5.1 ± 2.0 Ω. In comparison, the end-to-end resistance of a 7.5 cm yarn was 43 ± 5.9 Ω. As expected, the interlooping structure provided additional pathways for electron transport, resulting in reduced resistance relative to a single freestanding yarn.

Next, textile supercapacitors were knitted by feeding MXene-coated yarns into the machine through two yarn feeders; one feeder knitted one electrode, and the other feeder knitted the second electrode. A polyester yarn was knitted between the two yarn electrodes to prevent electrical shorting (Fig. 3a). Polyester was specifically chosen due to its hydrophilicity, which was important for conducting electrochemical tests in an aqueous electrolyte. Several device designs were programmed and knitted using this arrangement of yarn feeders. Following textile terminology, columns of knitted loops are referred to as wales and rows are referred to as courses, as indicated in Fig. 3a. The supercapacitor designs knitted included a vertical striped supercapacitor, in which two parallel wales of MXene-coated yarn electrodes were knitted (Fig. S5a), a horizontal striped supercapacitor, where two parallel courses of MXene-coated yarn electrodes were knitted (Fig. S5b), and an interdigitated device, the standard design for planar microsupercapacitors (Fig. S5c). It should be noted that for all samples, irrespective of fiber type or geometry, the machine parameters including stitch values, machine gauge, tension, and speed of knitting were held constant. To understand and optimize the performance of knitted supercapacitors, two distinct features of the textile device were investigated: the geometry, meaning the number of knit stitches within and between electrodes, and the knit structure. Many knit structures can be fabricated by a combination of stitch types that create patterns, resulting in textiles with different densities and dimensionalities.

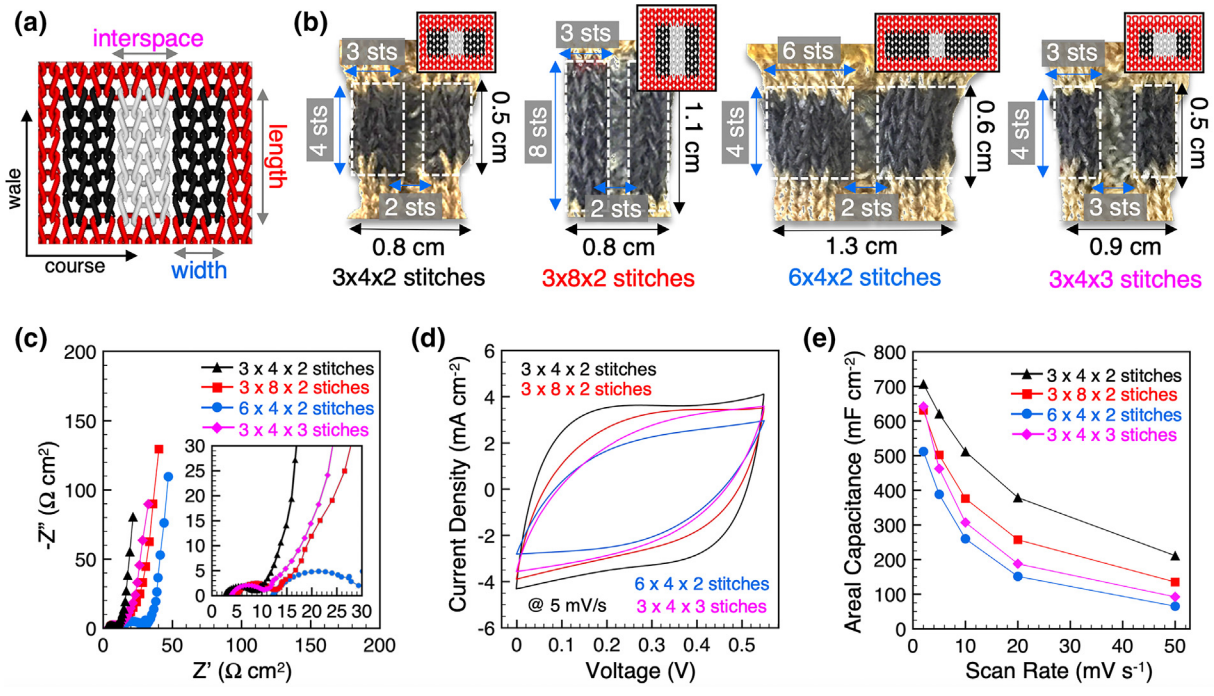

FIGURE 3

Knit geometry (length and width of electrodes and spacing between electrodes). (a) knit simulation depicting the structure and geometry of a vertical striped supercapacitor. Black yarns represent MXene-coated yarn electrodes, grey yarn represents an insulating yarn (polyester) analogous to a separator for on-chip microsupercapacitors, and red yarn represents a non-conductive yarn, (b) images of devices knitted with four different geometries, from left to right: standard device ("3 × 4 × 2 stitches"), double the number of stitches (sts) per wale ("3 × 8 × 2 stitches"), double the number of stitches per course ("6 × 4 × 2 stitches"), and increased spacing between electrodes by an additional stitch ("3 × 4 × 3 stitches"), (c) normalized Nyquist plots, (d) CV curves at 5 mV s^{-1}, (e) Areal capacitance as a function of scan rate. Devices tested in 1 M H_3PO_4.

In this work, different patterns were explored to understand the effect of knit structure on electrochemical performance.

Knit device geometry

For simplicity, the vertical striped device configuration was selected to study the effects of device geometry, namely the length and width of electrodes and the spacing between electrodes, on electrochemical performance. While these geometric parameters have been thoroughly studied for planar microsupercapacitors, knitted devices have additional manufacturing constraints which limit the achievable dimensions and resolution. For example, it has been shown for planar microsupercapacitors that the rate capability, power response, and energy density improve with narrow interspacing (space between electrodes) [41]. For these devices, the interspacing is typically less than 500 μm and closer to 100–300 μm for spray coated and printed devices [42,43]. However, for knitted devices, the minimum spacing between electrodes is largely dictated by the size of a knit loop. For 2-ply MXene-coated cotton yarns knitted on a 15-gauge knitting machine, the height of a loop was approximately 1.60 mm and width of a loop was 1.16 mm (Fig. S6a). As such, for vertical striped devices, the minimum interspace was ~1.2 mm (more than twice that of planar microsupercapacitors) (Fig. S6b). This limitation inherently poses challenges to designing knitted supercapacitors with high rate performance because the ion diffusion pathway is long. Thus, it is important to not only understand how geometric parameters affect the performance of these textile devices, but also to explore methods to minimize the interspacing while preventing the device from shorting. It should be noted that for initial characterization of electrochemical performance, supercapacitors were tested in aqueous electrolyte (1 M H_3PO_4) (Fig. S6c). After investigation of various device designs, PVA-H_3PO_4 gel electrolyte was used to better mimic practical applications of these devices.

The smallest device knitted, shown in Fig. 3b, consisted of two vertical stripes of MXene-coated yarn electrodes, where each stripe contained three wales of four stitches, with two wales of polyester loops between electrodes, and referred to as "3 × 4 × 2 stitches". The approximate MXene loading per geometric device area (0.5 cm × 0.8 cm) was 22.5 mg cm^{-2}. To our knowledge, this loading is higher than dip-coated fabrics reported in literature, which have active mass loadings in the range of 0.6–12 mg cm^{-2} (Table S3).

To study the effect of electrode length and width on device performance, the length was increased by doubling the number of stitches in each wale from 4 stitches to 8 stitches, subsequently referred to as "3 × 8 × 2 stitches" (Fig. 3b). To study the effect of electrode width on electrochemical performance, the number of stitches in each row was doubled from 3 stitches to 6 stitches, referred to as "6 × 4 × 2 stitches" (Fig. 3b). By doubling the device length, the length of yarn used to knit each electrode doubled from approximately 7.5 cm (~4.5 mg of MXene per electrode) to 13 cm (~7.8 mg of MXene per electrode), and the resistance across each knit electrode, measured diagonally across the electrode, increased from 5.1 ± 2.0 Ω to 11.6 ± 3.0 Ω using 2-ply MXene-coated cotton yarn as electrodes. Similarly, by doubling the device width, the length of yarn used to knit each electrode increased to approximately 15 cm and the resistance across each electrode increased to 10.9 ± 0.7 Ω. In addition to increasing the length and width of the electrodes, we increased the spacing between electrodes by adding an additional stitch between the electrodes, resulting in an increase in spacing from approximately 1 mm to 2 mm, referred to as "3 × 4 × 3 stitches" (Fig. 3b).

The Nyquist plots of these four devices obtained using electrochemical impedance spectroscopy (EIS) are shown in Fig. 3c. All of the devices show a small semicircle in the high-frequency region, except for the increased width device (6 × 4 × 2 stitches). This devices shows a more significant semicircle, corresponding to an increase in the interfacial charge transfer resistance. In the mid-frequency region, the length of the 45° slope is indicative of the length of the ion transport pathway during charging and discharging [42]. The increased spacing device (3 × 4 × 3 stitches) showed a longer 45° slope in this region than the 3 × 4 × 2 device, due to the additional stitch of polyester between the two electrodes, which increased the length of the ion diffusion pathway. Interestingly, the increased length device (3 × 8 × 2 stitches) showed a similar profile in the mid-frequency frequency region. We hypothesize that when the length of the electrodes increased, the difference in mechanical properties between the MXene-coated cotton yarn and the surrounding non-conducting yarn resulted in the fabric relaxing in such a way that the spacing between electrodes increased relative to the 3 × 4 × 2 stitches device. As such, the ion diffusion path for the 3 × 8 × 2 device increased relative to the 3 × 4 × 2 device, which was reflected in the Nyquist plots. In the low frequency region, a vertical line is indicative of the behavior of an ideal capacitor. All of the devices show a near-vertical line in this region, with the increased spacing device (3 × 4 × 3 stitches) showing a slight decrease in slope.

Cyclic voltammograms (CVs) were recorded from 2 mV s^{-1} to 50 mV s^{-1} in the range of 0 to 0.55 V in 1 M H_3PO_4 to characterize the capacitive behavior of the four devices. The CVs were quasi-rectangular for the 3 × 4 × 2 device up to 20 mV s^{-1} (Fig. S7a), while the CVs for the other devices deviate further from this shape at lower scan rates (Fig. S7b–d). As shown in Fig. 3d, the enclosed area is visibly larger for the 3 × 4 × 2 device at 5 mV s^{-1} compared with the other three devices, indicating better energy storage capability. For all of the devices, the Coulombic efficiency was >93% at all scan rates. Fig. 3e summarizes the areal capacitances of the devices at scan rates from 2 mV s^{-1} to 50 mV s^{-1}. The 3 × 4 × 2 device outperformed the other geometries in terms of areal capacitance, reaching 707 mF cm^{-2} at 2 mV s^{-1} (566 mF cm^{-1}, 31 F g^{-1}) and 211 mF cm^{-2} at 50 mV s^{-2}. It should be noted that the capacitance for the increased length device (3 × 8 × 2 stitches) was the highest at all scan rates before normalization (305 mF at 2 mV s^{-1} compared with 155 mF at 2 mV s^{-1} for the 3 × 4 × 2 device), due to the greater total amount of MXene present. The increased width device (6 × 4 × 2 stitches) also had a greater amount of MXene compared with the 3 × 4 × 2 device, however, it is likely that not all of the MXene was accessible due to the long diffusion pathway. Overall, larger spacing between electrodes resulted in lower areal capacitance at each scan rate, following trends of planar microsupercapacitors [41,44]. The

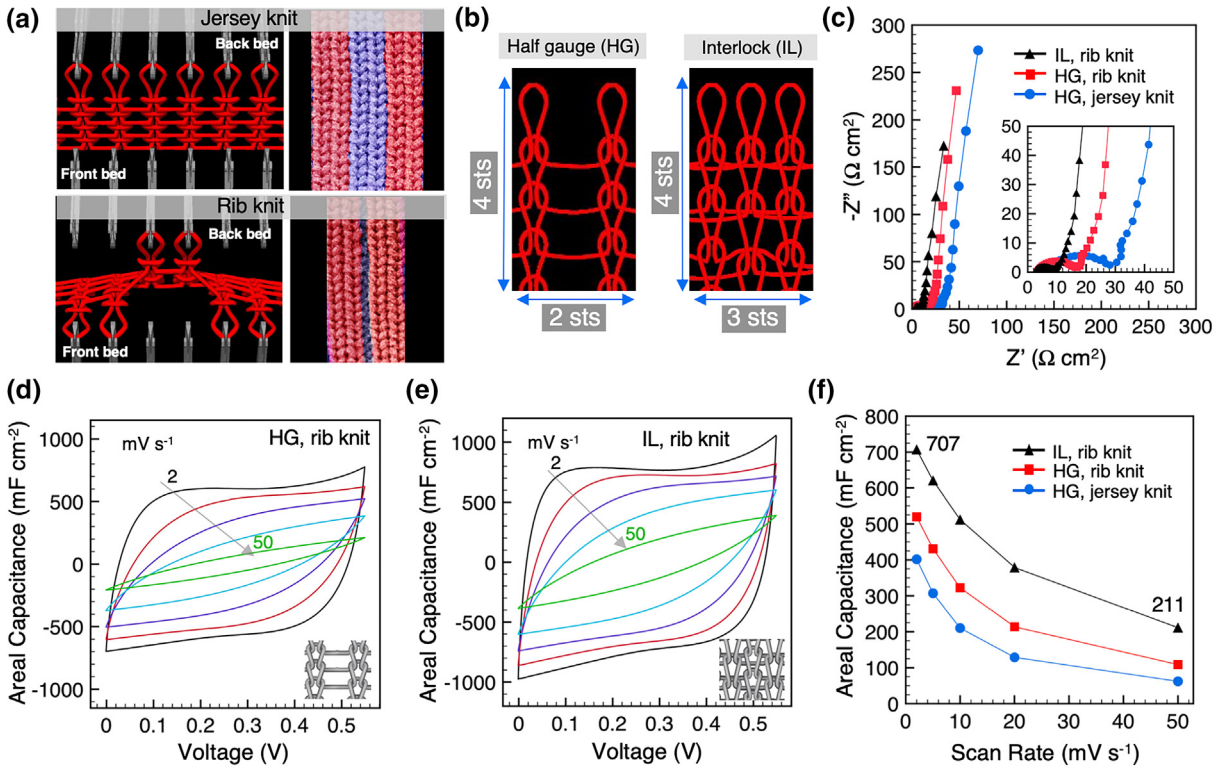

FIGURE 4

Knit structure (jersey knit *vs.* rib knit and half-gauge *vs.* interlock). (a) Knit simulations (left) and false-colored images (right) of jersey knit (top) and rib knit (bottom) fabrics, (b) knit simulations of electrodes knitted using half-gauge and interlock stitch patterns. sts = stitches, (c) normalized Nyquist plots of devices knitted with the half-gauge (HG) stitch pattern and interlock (IL) stitch pattern and devices knitted into jersey knit and rib knit structures, (d) CV curves at different scan rates (2, 5, 10, 20, 50 mV s^{-1}) for a half-gauge rib knit device, (e) CV curves at different scan rates (2, 5, 10, 20, 50 mV s^{-1}) for an interlock rib knit device, (f) Areal capacitance as a function of scan rate for devices knitted with different stitch patterns. Devices tested in 1 M H_3PO_4.

3x4x2 device demonstrated the highest areal capacitance and this geometry was selected for further studies.

Device knit structure

After optimizing the device geometry, specifically the number of stitches per electrode and between electrodes, the effect of knit structure on electrochemical performance was studied. The most basic knit structure, known as a jersey knit, is created using one kind of stitch and all of the stitches lie on one bed of knitting needles (Fig. 4a). A more dimensional structure, the rib knit, is created using a specific pattern of two kinds of stitches, which lie on the front and back needle beds. These two structures, jersey and rib, are among the most widely used structures in knitted textiles. We hypothesized that the dimensionality and curling behavior of these structures could be exploited to further reduce the spacing between electrodes and improve the diffusion kinetics and overall performance of knitted supercapacitors.

To fabricate jersey supercapacitors, the electrodes and the separator yarn were knitted on the same bed of knitting needles. To create rib supercapacitors, the electrodes were knitted on the front bed of needles and the separator was knitted on the back bed of needles. After the devices were knitted and given time to relax (Fig. S8a), there was a clear difference in the dimensionality of the structures. As shown in Fig. S8b, the cross-section of the jersey device was flat and planar, while the rib knit device had a cavity between the two electrodes. To prevent the devices from shorting, two stitches of separator yarn were required between the two electrodes for all knit geometries and structures tested. Interestingly, while the number of stitches between electrodes was held constant, the spacing between electrodes was approximately 600 μm for the rib knit device and 2.8 mm for the jersey knit device (Fig. S8c). This difference in spacing can be attributed to the natural relaxation of the fabrics, which is dictated by their knit structure. It has been shown that a curling behavior occurs at the boundary condition between front bed stitches and back bed stitches [45]. As such, for the rib knit device, the MXene coated yarns, which were knitted on the front bed of needles, curled in towards each other, while the separator yarn, which was knitted on the back bed of needles, tucked behind the electrodes. In doing so, the spacing between electrodes was minimized.

In addition to knitting both rib and jersey structures, electrodes were knitted using half-gauge and interlock stitch patterns. A half-gauge structure is knitted using every other needle on the needle bed. An interlock structure is created by first knitting every other needle on the bed, and then going back and knitting the skipped needles. As a result, the interlock stitch pattern produces a denser textile than the half-gauge stitch pattern. Electrodes knitted using the interlock stitch pattern consisted of 3 wales and 4 courses and electrodes knitted using the half-gauge stitch pattern consisted of 2 wales and 4 courses (Figs. 4b and S8a). Since the interlock stitch pattern used one additional knit-

ting needle per course, these devices required approximately 7.5 cm of MXene-coated yarn per electrode (4.5 mg per electrode when knitting 2-ply MXene-coated cotton yarns), in comparison to ~6.5 cm of yarn per electrode for the half-gauge devices (3.9 mg per electrode).

The Nyquist plots of three devices knitted with different stitch patterns and structures (half-gauge jersey knit, half-gauge rib knit, and interlock rib knit) are shown in Fig. 4c. Comparing rib knit and jersey knit devices (both knitted using the half-gauge stitch pattern), the rib knit supercapacitor (HG, rib knit) had a smaller semi-circle in the high-frequency region and lower resistance compared with the jersey knit device (HG, jersey knit). The interlock rib knit device (IL, rib knit) showed the smallest semicircle and lowest resistance of the three devices.

Representative CV profiles at scan rates from 2 mV s^{-1} to 50 mV s^{-1} in 1 M H_3PO_4 are shown for each device in Figs. 4d, e, and S8d. The CV curves for the half-gauge rib knit device were quasi-rectangular up to 10 mV s^{-1} (Fig. 4d) and up to 20 mV s^{-1} for the rib knit interlock device (Fig. 4e). The rate performance of the half-gauge jersey device was poor, showing distorted CVs at 5 mV s^{-1}, indicating high resistance. As such, the areal capacitance for this device was low, only reaching 402 mF cm^{-2} at 2 mV s^{-1}, shown in Fig. 4f. Therefore, the rib structure was considered for the remainder of this work. The interlock rib knit device (IL, rib knit) achieved the highest areal capacitance, 707 mF cm^{-2} at 2 mV s^{-1}, approximately 36% greater than the half-gauge rib knit (HG, rib knit) device at 2 mV s^{-1} (520 mF cm^{-2}) and up to almost double the areal capacitance at 50 mV s^{-1} (211 mF cm^{-2} vs. 109 mF cm^{-2}). This increase in capacitance can be attributed to the difference in MXene loading per unit area, from approximately 19.5 mg cm^{-2} to 22.5 mg cm^{-2} for half-gauge and interlock rib knit devices, respectively. Additionally, the improvement in rate performance can be attributed to the increased number of loops per unit area. The interlock structure has more loops of MXene-coated yarn than the half-gauge device within approximately the same area (12 loops/electrode for the interlock device *vs.* 8 loops/electrode for the half-gauge device), providing more electrical connections per electrode. In sum, a denser fabric results in higher areal capacitance and better rate performance compared with a porous fabric.

Electrode yarn selection

The versatility of 3D knitting enables the same device to be knitted with a variety of yarns after developing a knit program and defining the relevant machine parameters (stitch tightness, knitting speed, etc.). After the interlock rib knit supercapacitor was designed, programmed, and tested using 2-ply MXene-coated cotton yarns as electrodes, the same structure was knitted using MXene-coated nylon fibers to further validate this new textile supercapacitor architecture. However, the MXene mass loading (mg cm^{-1}) on the nylon fibers was lower than that on the 2-ply cotton yarn and since capacitance scales linearly with MXene loading [14], this would be seen as a deterrent for using MXene-coated nylon fibers in fiber and yarn-based supercapacitor applications. As such, most reports in literature have focused on MXene-coated natural fibers for this purpose [34,46–48]. However, we expected that knitting could be used as a tool to increase the mass loading of a device per unit area by plying MXene-coated yarns together and feeding them into the knitting machine as if they were a single yarn, a technique called "co-knitting". In doing so, the capacitance per area can be doubled or even tripled by co-knitting 2 or 3 yarns together, respectively.

To demonstrate the potential of co-knitting to improve device capacitance, 1-ply of cotton yarn and 1-ply of nylon multifilament fibers were coated with MXene such that the mass loading was 0.3 mg cm^{-1} (53 wt.%) for 1-ply cotton yarns and 0.22 mg cm^{-1} (41 wt.%) for 1-ply nylon fibers. Devices were knitted by feeding 1 end or 2 ends of each of these MXene-coated fibers/yarns into the electrode yarn feeders. It should be noted that the stitch value, a machine parameter which controls the tightness of each stitch, was kept constant for all samples, resulting in loose loops made from 1-ply electrodes (Fig. 5a).

As shown in Fig. 5b, the Nyquist plots for 1 end of MXene-coated cotton yarn (1-MX-Cot) and 2 ends of MXene-coated cotton yarn (1-MX-Cot-2) are almost identical in the high frequency region, but the resistance is larger in the low frequency region for the device knitted with 1 end. The resistance measured diagonally across an electrode was ~18 Ω and ~9.8 Ω for devices made using 1 end of MXene-coated cotton yarn and 2 ends of MXene-coated cotton yarn, respectively. While the mass loading for 1-ply MXene-coated cotton yarn was only 0.3 mg cm^{-1}, the CV profiles tested in 1 M H_3PO_4 (Fig. 5c) are still quasi-rectangular up to 20 mV s^{-1}, like 2-ply MXene-coated cotton yarns (2-MX-Cot) with higher mass loading (0.6 mg cm^{-1}). The areal capacitance of the device knitted with 2 ends of 1-ply MXene-coated cotton (1-MX-Cot-2) was 765 mF cm^{-2} at 2 mV s^{-1}, compared to 332 mF cm^{-2} for the device knitted with 1 end of MXene-coated cotton (1-MX-Cot) (Fig. 5d). Furthermore, co-knitting 2 ends of 1-ply MXene-coated cotton yarns together each with MXene loading of 0.30 mg cm^{-1} resulted in nearly identical electrochemical behavior to devices knitted using 2-ply MXene-coated cotton yarn as electrodes. This is important because it confirms that a single yarn can be coated fewer times and subsequently plied and co-knitted to achieve the same result as coating multi-ply yarns many times. As such, this technique can be used to significantly reduce the number of coating cycles and ultimately the duration of coating.

The same method was followed for MXene-coated nylon fibers; devices were knitted using 1 end of MXene-coated nylon multifilament fibers (1-MX-Nyl) and 2 ends of 1-ply MXene-coated nylon multifilament fibers (1-MX-Nyl-2), as shown in Fig. 5e. The Nyquist plots reveal the same behavior as for MXene-coated cotton yarns. The diameter of the semi-circle in the high frequency region is similar for devices made with 1 end of MXene-coated nylon fibers and 2 ends of 1-ply MXene-coated nylon fibers (1-MX-Nyl-2), while the resistance is larger in the low frequency region for the device knitted with 1 end of MXene-coated nylon fibers (Fig. 5f). The CV curves for devices made with 1 end of MXene-coated nylon fibers are resistive (Fig. S9), while devices made with 2 ends of MXene-coated nylon fibers show more rectangular profiles at low scan rates (Fig. 5g). In general, the nylon-based devices were more resistive than the cotton-based devices, which is likely due to two reasons. First, 1 end of 1-ply MXene-coated nylon fibers was finer than 1 end of 1-ply MXene-coated cotton yarn, resulting in loose

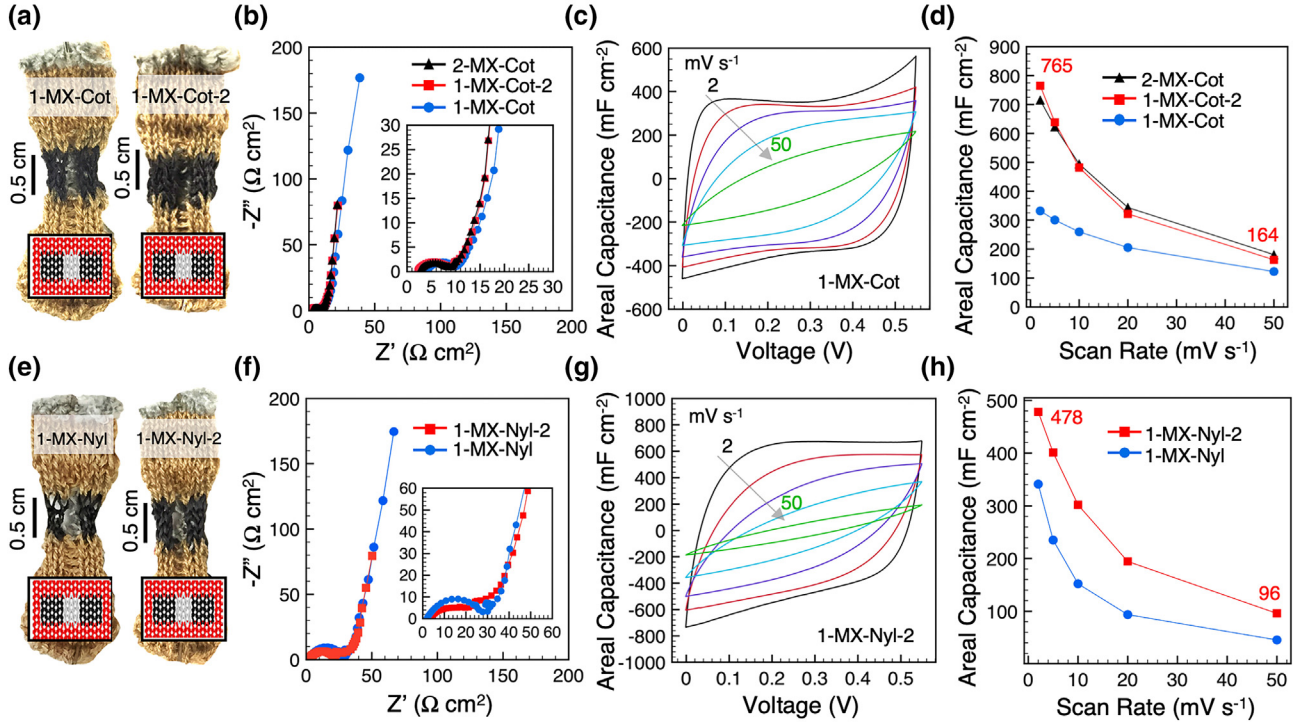

FIGURE 5

Electrochemical performance of knitted devices using MXene-coated cotton and MXene-coated nylon fibers as electrodes. (a) images of devices knitted with 1 end (1-MX-Cot) and 2 ends (1-MX-Cot-2) of 1-ply MXene-coated cotton yarns, (b) Normalized Nyquist plots of MXene-coated cotton devices, including a device made using 2-ply MXene-coated cotton yarns (2-MX-Cot), (c) CV curves at different scan rates (2, 5, 10, 20, 50 mV s^{-1}) of a device knitted with 1 end of MXene-coated cotton yarn, (d) Areal capacitance of MXene-coated cotton devices as a function of scan rate, (e) images of knitted supercapacitors with 1 end (1-MX-Nyl) and 2 ends (1-MX-Ny-2) of 1-ply MXene-coated nylon fibers as electrodes, (f) normalized Nyquist plots of MXene-coated nylon devices; (g) CV curves at different scan rates (2, 5, 10, 20, 50 mV s^{-1}) for a device made with 2 ends of MXene-coated nylon, (h) areal capacitance as a function of scan rate for MXene-coated nylon devices. Devices tested in 1 M H_3PO_4.

loops at the selected stitch value and poor connectivity between loops. Additionally, the spacing between electrodes was ~500 μm larger for nylon devices compared with cotton devices (for both 1-ply and 2 ply devices), even though the knit program and machine parameters were held constant. Thus, to improve the performance of nylon-based devices, the stitch tightness needs to be further optimized to improve loop connectivity and spacing between electrodes. The capacitance of devices made with 2 ends of MXene-coated nylon fibers reached 478 mF cm^{-2} at 2 mV s^{-1} (Fig. 5h).

Knitted supercapacitors

For use in wearable applications, the interlock rib knit supercapacitors made using 2-ply MXene-coated cotton yarns were tested in PVA-H_3PO_4 gel electrolyte. As shown in Fig. 6a, the CV curves were quasi-rectangular and the Nyquist plot in Fig. 6b shows a small semi-circle in the high frequency region and low resistance in the low frequency region. The galvanostatic charge–discharge (GCD) curves at different current densities, shown in Fig. S10a, show a small *iR* drop (~0.06 V at 0.875 mA cm^{-2}). The areal capacitance reached 519 mF cm^{-2} at 2 mV s^{-1} and 321 mF cm^{-2} at 10 mV s^{-1} (Fig. S10b). The device was tested over 10,000 charge–discharge cycles and showed >100% capacitance retention and Coulombic efficiency of ~100% at all cycles (Fig. 6c), indicating excellent cycling stability. We expect that the increased capacitance with cycling is due to the slow penetration of the gel electrolyte into the electrodes, which resulted in improved capacitance with cycling. The Ragone plot shows a maximum areal energy density and areal power density of 25.4 μWh cm^{-2} and 0.47 mW cm^{-2}, respectively, which are comparable to those of fabric-based supercapacitors reported in literature (Fig. S10c).

Using computer-aided knitting, multiple devices were designed, simulated, and knitted in series, shown in Fig. 6d, and in parallel. With three devices connected in series, the voltage window reached 1.5 V (Fig. 6e) and in parallel, the current increased with the number of devices connected (Fig. 6f). The ease of scalable manufacturing of knitted supercapacitors using programmable knitting technology demonstrates promise for MXene-coated yarns to be used as electrodes in textile-based devices. Employing similar techniques used in this work, other devices, such as antennas and sensors, could potentially be knitted into textiles and connected to these knitted supercapacitors to create fully integrated circuits.

Conclusion

Developing an automated yarn-coating platform to produce meters of MXene-coated cotton and nylon yarns enabled the rapid prototyping of knitted supercapacitors, a critical step towards understanding and optimizing the performance of this new device architecture. The coating method developed was sim-

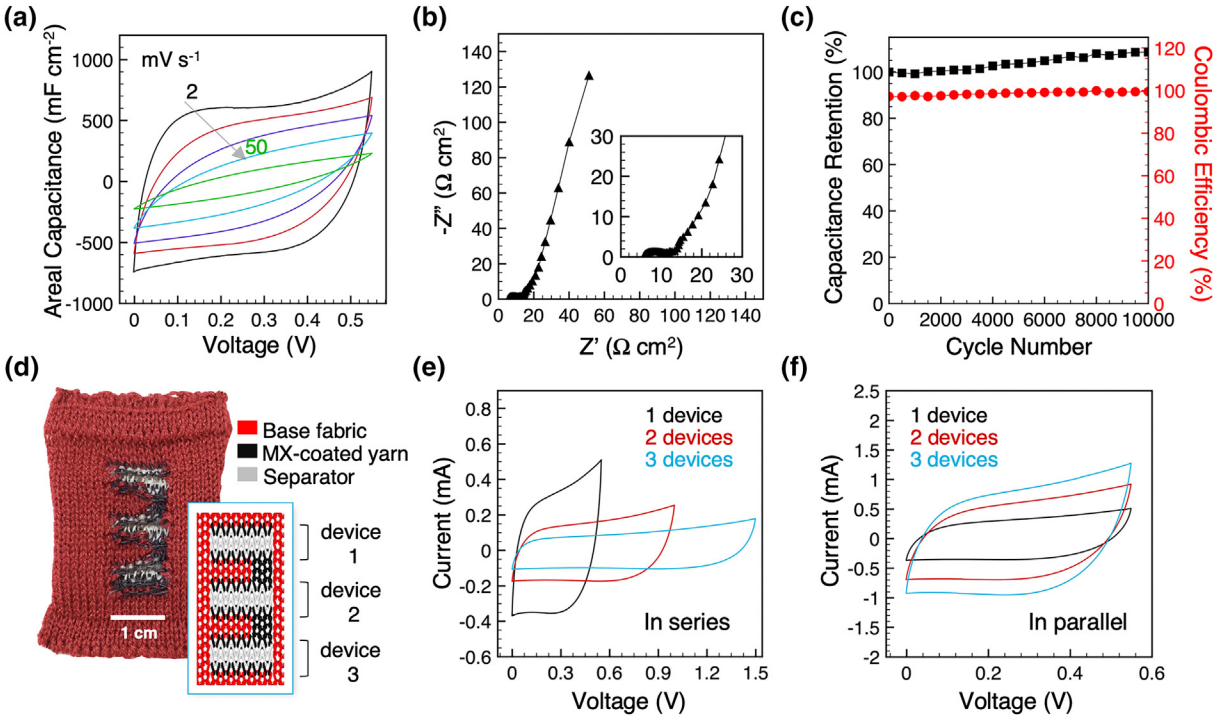

FIGURE 6

Devices tested in PVA-H_3PO_4 gel electrolyte. (a) CV curves at different scan rates (2, 5, 10, 20, 50 mV s^{-1}), (b) normalized Nyquist plot, (c) cycling stability over 10,000 cycles at 20 mV s^{-1}, (d) Optical image and simulation of three devices knitted in series, CV curves at 5 mV s^{-1} of multiple devices connected in (e) series, and (f) parallel.

ple, efficient, and scalable, eliminating the time and labor-intensive process of manual dip-coating. With only 10 m of MXene-coated yarn, ~66 supercapacitors could be knitted. The electrochemical performance of the produced knit devices was optimized by tuning the device geometry (length and width of electrodes and spacing between electrodes) and knit structure. We determined that the larger the spacing between electrodes and the length/width of the electrodes, the smaller is the areal capacitance at each scan rate. While the spacing between electrodes was largely dictated by the size of a knit loop, the knit structure was modified to further minimize this spacing with a 4 fold reduction in the spacing between electrodes from approximately 2.8 to 0.6 mm, increasing the areal capacitance from 402 to 707 mF cm^{-2} at 2 mV s^{-1}. In addition to knit geometry, stitch density played a significant role in device performance; denser fabrics had higher areal capacitance and better rate performance than porous fabrics due to improved connectivity between loops and increased MXene-loading per geometric area. The optimized device, interlock rib knit (3 × 4 × 2 stitches), knitted using 2-ply MXene-coated cotton yarns as electrodes, demonstrated cycling stability over 10,000 cycles in gel electrolyte and delivered energy and power densities of 25.4 μWh cm^{-2} and 0.47 mW cm^{-2}, respectively.

This new device architecture was further validated by using other MXene-coated yarns as electrodes. While synthetic fibers are often more difficult to load with active material relative to most natural fibers, knitting can be used as a tool to expand the library of fibers and yarns chosen as substrates for wearable electrode materials by plying fiber/yarn electrodes together, which on their own have lower active mass loading. As long as the pristine fiber/yarn meets the requirements of hydrophilicity and knittability, it has the potential to be used as a substrate for MXene-based knitted electrodes.

Future efforts are needed to improve the rate performance of these knitted devices, for instance, twisting the MXene-coated yarn electrodes with a fine conductive commercial yarn to act as a current collector. Additionally, the long-term stability and safety of the device can be improved by encapsulating the device, potentially using a thin polymer coating over the knitted textile. At its present stage, this work represents a major step towards the mass production of knittable conductive yarns and wearable energy storage devices and the potential for use in practical applications.

Experimental section

Synthesis of MXene

The synthesis of $Ti_3C_2T_x$ MXene has been previously reported [31,49]. Briefly, 3 g of Ti_3AlC_2 MAX phase (Carbon-Ukraine) with mesh size ~≤45 μm was slowly added to 60 mL of etchant containing 12 M HCl (Alfa Aesar, 98.5%), deionized water, and 49% HF (Acros Organics) in a volumetric ratio of 6:3:1, respectively. This solution was stirred on a hot plate at 300 rpm for 24 h at room temperature. After etching, the multilayer $Ti_3C_2T_x$ MXene was washed repeatedly with deionized water by centrifugation at 3500 rpm for 2–6 min until the pH reached 6–7. For delamination, the multilayer MXene was mixed with 1 g of LiCl in 50 mL of deionized water, followed by manual shaking for up

to 2 min. Next, the solution was stirred at room temperature at 400 rpm for 4 h. After stirring, the MXene solution was washed twice with deionized water by centrifugation at 3500 rpm for 1 min, followed by centrifugation at 3500 rpm for up to 1 h (until the supernatant was clear). To separate unreacted MAX from MXene, the sediment was dispersed in deionized water and repeatedly centrifuged at 3500 rpm for 4 min. The supernatant, which consisted of MXene (unreacted MAX remains at the bottom of the centrifuge tube), was collected during each cycle. For coating yarns, the collected supernatant was centrifuged at 9000 rpm for 25 min to concentrate the MXene solutions. The delaminated MXene was collected and re-dispersed in deionized water. The concentration of the dispersions was measured by filtering a known volume of solution (1–2 mL) through a polypropylene filter with a pore size of 64 nm (Celgard, LLC). The mass was recorded after the film was dried overnight under vacuum. The MXene concentration used for yarn coating ranged from 10 to 15 mg mL^{-1}. Before coating, MXene dispersions were probe sonicated in a cooling chamber at a temperature of −9 °C for 20 min at an amplitude of 50% and pulse ratio of 80/20.

Automated yarn coating

One-ply cotton yarn (~250 denier) was supplied by the Commonwealth Scientific and Industrial Research Organization (CSIRO) and multifilament nylon 6 fibers (27 filaments per bundle) were melt-spun at Deakin University (Geelong, Australia). Single ends of cotton yarns were plied and twisted together using an automated twisting machine (DirecTwist, Agteks) to produce 2-ply cotton yarn. The twist was set to 150 T m^{-1}.

A custom built wet-spinning machine (Dissol Pty. Ltd) was modified to coat the yarns with MXene. Pristine yarns were passed through a series of four baths of MXene which were placed along the wet-spinning line. The baths, made from vinyl tubing (inner diameter: 6 mm, length: 9 cm), were each filled with approximately 4 mL of the MXene/water dispersion (90% of flakes ~150 nm) and were placed 3 m apart along the coating line. The rollers were set to a speed of 0.4 m min^{-1} and the coated yarn was collected onto a yarn winder after passing through the four baths. The process was repeated until the desired MXene mass loading was achieved (0.6 mg cm^{-1} for 2-ply cotton yarns and 0.22 mg cm^{-1} for multifilament nylon fibers).

3D knitting

Knitted supercapacitor devices were programed and simulated using Shima Seiki's SDS-ONE APEX3 design system. Devices were knitted on a Shima Seiki 15-gauge SWG-041N knitting machine. MXene-coated yarns were knitted at a stich value of 36 and a speed of 0.03 m s^{-1}. A single ply of polyester yarn (REPREVE) was knitted between the two MXene-coated yarn electrodes to prevent the devices from electrical shorting. The polyester yarn was knitted at a stitch value of 32 and a speed of 0.10 m s^{-1}. The yarn used to knit the fabric outside of the supercapacitor devices were a blend of nylon (85%) and modal fibers (15%) (Silk City Fibers).

Supercapacitor assembly

Knitted devices were tested in both aqueous (1 M H_3PO_4) and gel (1 M H_3PO_4/PVA) electrolytes. The gel electrolyte was prepared by dissolving 3 g of PVA (Sigma-Aldrich, MW = 89,000 Da) in 30 mL of water at 80 °C and stirring for up to 4 h. The solution was removed from the hotplate and allowed to cool completely before adding 3 g of concentrated phosphoric acid (EMD Millipore Corporation). All knitted devices were stored overnight under vacuum before addition of electrolyte for electrochemical testing. For testing in aqueous electrolyte, stainless steel alligator clips or stainless-steel rivets were connected to the fabric and the devices were placed in a plastic bag filled with the electrolyte. The alligator clips were connected directly to the potentiostat. For testing in gel electrolyte, the gel was placed drop-wise onto the fabric and the devices were dried in air.

Electrochemical measurements

The following electrochemical tests, cyclic voltammetry (CV), electrochemical impedance spectroscopy (EIS), and galvanostatic charge–discharge (GCD) were conducted using a VMP3 electrochemical workstation (BioLogic). EIS was performed in the frequency range of 200 kHz–2 mHz at open circuit potential by applying a sinusoidal potential signal with an amplitude of 10 mV. The current densities shown in the GCD curves were normalized by the geometrical footprint area of the knitted devices. GCD curves were recorded from 0.5 mA cm^{-2} to 2.0 mA cm^{-2} and CVs were recorded at the following scan rates: 2, 5, 10, 20, and 50 mV s^{-1}. The areal capacitance of a knitted device was calculated by integrating the discharge current of the cyclic voltammograms with respect to time, according to the following equation

$$C_A(\text{mF cm}^{-2}) = \left(\int_0^t i dt\right)/(V \times A); \quad (1)$$

where C_A is the specific capacitance normalized to the geometric area of the device, t is the discharge time, i is the discharge current (mA), V is the voltage window, and A is the geometric area of the device (cm^2). The gravimetric capacitance (F g^{-1}) of the devices was calculated based on the mass of the active material and the length-specific capacitance (mF cm^{-1}) was calculated based on the length of the electrodes.

For electrochemical cycling, the devices were cycled up to 10,000 cycles at 20 mV s^{-1}. The capacitance retention (C_{Ret}) of the device was calculated by normalizing the capacitance at each cycle (C_i) by the capacitance at the first cycle (C_1), according to the following equation

$$C_{Ret} = (C_i/C_1) \times 100\% \quad (2)$$

The areal energy density (E_A) and areal power density (P_A) were calculated using the following equations

$$E_A(\mu\text{Wh cm}^{-2}) = 0.5 C_A V^2 \quad (3)$$

$$P_A(\text{mW cm}^{-2}) = E_A/t \quad (4)$$

where t is the discharge time.

Characterization

Yarns and knitted fabrics were imaged with a field emission scanning electron microscope (FESEM Zeiss VP5 Supra). The samples

were sputter coated with platinum/palladium at 40 mA for 40 s (Cressington Scientific 108 Auto) to avoid charging issues while imaging. Depth profile images were taken using a digital microscope (Keyence VHX-600 Series). X-ray diffraction (XRD) patterns were acquired using a powder diffractometer (Rigaku Smart Lab) using Cu K_α radiation ($\lambda = 1.5406$ Å) at a step size of 0.03° with 0.5 s dwell time. All samples were dried at ambient temperatures before characterization. X-ray photoelectron spectroscopy (XPS) measurements were carried out on a PHI VersaProbe 5000 instrument (Physical Electronics) using a 50 W monochromatic Al-K_α X-ray (1486.6 eV) beam with a 200 μm spot size. Charge neutralization was applied using a dual beam setup irradiating low energy Ar^+ ions and electrons. Samples were sputtered using Ar^+-ion source at an accelerating voltage of 2 kV and current density of 0.5 μA mm^{-2} for up to 12 min using Zalar rotation technique. Survey spectra were collected using a pass energy of 117.4 eV and energy resolution of 0.5 eV and the core level region spectra were collected using a pass energy of 23.5 eV and energy resolution of 0.05 eV. Quantification and peak fitting were conducted using CasaXPS (V2.3.19). Binding energy scale correction was applied using the adventitious carbon C–C peak at 285.0 eV. Mixed Gaussian-Lorentzian GL(30) models were used for oxygen related species (eg. TiO_2) and asymmetric Lorentzian models LA(2,4,6) were used for metal related species (eg. Ti-C). Shirley model was used for background fitting. MXene flake size was measured by dynamic light scattering (DLS, Zetasizer Nano ZS, Malvern Panalytical). Five measurements were taken of each sample and the average value was reported. Yarn resistance was measured using a two-probe digital multimeter (Hyelec, MS8233D). Conductivity (σ) was calculated according to the following equation

$$\sigma = l/RA_C \tag{5}$$

where l, R, and A_c are the length, resistance, and the cross-sectional area of the yarn, respectively. The cross-sectional area was calculated using the diameter of a yarn, which was measured from SEM images.

CRediT authorship contribution statement

Ariana Levitt: Conceptualization, Investigation, Writing - original draft, Writing - review & editing. **Dylan Hegh:** Methodology, Investigation, Writing - review & editing. **Patrick Phillips:** Methodology, Writing - review & editing. **Simge Uzun:** Writing - review & editing. **Mark Anayee:** Investigation, Writing - review & editing. **Joselito M. Razal:** Conceptualization, Supervision, Writing - review & editing. **Yury Gogotsi:** Conceptualization, Supervision, Writing - review & editing. **Genevieve Dion:** Conceptualization, Supervision, Writing - review & editing.

Declaration of Competing Interest

The authors declare that they have no known competing financial interests or personal relationships that could have appeared to influence the work reported in this paper.

Acknowledgements

The authors would like to thank Dr. Narendra Kurra for guidance with electrochemical testing and Robert Lehrich and Amy Stoltzfus for their assistance with knit programming. A.L. and M.A. were supported by the National Science Foundation Graduate Research Fellowship under Grant No. DGE-1646737. Any opinion, findings, and conclusion or recommendations expressed in this material are those of the author(s) and do not necessarily reflect the views of the National Science Foundation. A.L. was also funded by the Australia-Americas PhD Research Internship Program. This work was performed in part at the Deakin University node of the Australian National Fabrication Facility. S.U. was sponsored by the Fluid Interface Reactions, Structures and Transport (FIRST) Center, an Energy Frontier Research Center (EFRC) funded by the U.S. Department of Energy, Office of Science, and Office of Basic Energy Sciences. J.M.R. acknowledges support from the Australian Research Council (FT130100380, IH140100018, and DP170102859). SEM, XRD, and XPS were performed at the Core Research Facilities (CRF) of Drexel University.

Data availability

The raw/processed data required to reproduce these findings cannot be shared at this time due to technical or time limitations.

Appendix A. Supplementary data

Supplementary data to this article can be found online at https://doi.org/10.1016/j.mattod.2020.02.005.

References

[1] S. Chen et al., Adv. Funct. Mater. 28 (2018) 1802547.
[2] Z. Liu et al., Adv. Mater. 30 (2018) 1704229.
[3] H. Kim et al., ACS Appl. Mater. Interfaces 10 (2018) 32760–32764.
[4] T. Jia et al., Adv. Funct. Mater. 29 (2019) 1808241.
[5] T. Hughes-Riley, T. Dias, C. Cork, Fibers 6 (2018).
[6] T.M. Fernandez-Carames, P. Fraga-Lamas, Electronics 7 (2018) 405–441.
[7] Z. Wang et al., Small 14 (2018) 1802225.
[8] J. Du et al., Adv. Funct. Mater. 28 (2018) 1707351.
[9] J.H. Kim et al., Sci. Rep. 8 (2018) 13309.
[10] J. Lv et al., Energy Environ. Sci. 11 (2018) 3431–3442.
[11] J. Chen et al., Nano Energy 50 (2018) 536–543.
[12] L. Zhang, W. Viola, T.L. Andrew, ACS Appl. Mater. Interfaces 10 (2018) 36834–36840.
[13] W. Zeng et al., Adv. Mater. 26 (2014) 5310–5336.
[14] J. Zhang et al., Nanoscale 9 (2017) 18604–18608.
[15] D. Zhang et al., ACS Nano 8 (2014) 4571–4579.
[16] Y. Ma et al., ACS Nano 9 (2015) 1352–1359.
[17] S. Zhai et al., Mater. Horiz. 2 (2015) 598–605.
[18] R. Vallet et al., SPIE Proc. 10194 (2017).
[19] K. Jost et al., Adv. Energy Mater. 5 (2015) 1401286.
[20] M. Tebyetekerwa et al., Energy Environ. Sci. 12 (2019) 2148–2160.
[21] T.L. Andrew et al., Acc. Chem. Res. 51 (2018) 850–859.
[22] C. Choi et al., Adv. Energy Mater. 6 (2016) 1502119.
[23] M. Naguib et al., Adv. Mater. 23 (2011) 4248–4253.
[24] B. Anasori, M.R. Lukatskaya, Y. Gogotsi, Nat. Rev. Mater. 2 (2017) 16098.
[25] C. (John) Zhang et al., Adv. Mater. 29 (2017). 1702678.
[26] M.R. Lukatskaya et al., Science 341 (2013) 1502–1505.
[27] M. Ghidiu et al., Nat. Lond. 516 (2014) 78–81.
[28] K. Maleski et al., ACS Appl. Mater. Interfaces 10 (2018) 24491–24498.
[29] T.H. Park et al., ACS Nano 13 (2019) 6835–6844.
[30] S. Seyedin, E.R.S. Yanza, J.M. Razal, J. Mater. Chem. A 5 (2017) 24076–24082.
[31] A.S. Levitt et al., J. Mater. Chem. A 7 (2019) 269–277.
[32] M. Hu et al., Adv. Mater. Technol. 2 (2017) 1700143.
[33] J. Zhang et al., Small 15 (2019) 1804732.
[34] S. Uzun et al., Adv. Funct. Mater. 29 (2019) 1905015.

[35] C.E. Shuck et al., Adv. Eng. Mater. (2020) 1901241.
[36] M. Alhabeb et al., Chem. Mater. 29 (2017) 7633–7644.
[37] P. Louette, F. Bodino, J.-J. Pireaux, Surface Sci. Spectra 12 (2005) 12–17.
[38] R.J.J. Jansen, H.V. Bekkum, Carbon 33 (1995) 1021–1027.
[39] J.R. Pels et al., Carbon 33 (1995) 1641–1653.
[40] D. Jaeger, J. Patscheider, Surface Sci. Spectra 20 (2013) 1–8.
[41] W. Liu et al., ACS Nano 9 (2015) 1528–1542.
[42] Y.-Y. Peng et al., Energy Environ. Sci. 9 (2016) 2847–2854.
[43] H. Hu, T. Hua, J. Mater. Chem. A 5 (2017) 19639–19648.
[44] S.-K. Kim et al., Adv. Mater. 26 (2014) 5108–5112.
[45] C. Knittel, Tools to Predict and Understand the Self-folding Behavior of Knitted Textiles, Doctoral Dissertation, Drexel University, 2019.
[46] L. Geng et al., Cellulose 26 (2019) 2833–2847.
[47] T. Li et al., J. Mater. Chem. C 7 (2019) 1022–1027.
[48] J. Yan et al., RSC Adv. 8 (2018) 39742–39748.
[49] A. Sarycheva et al., Sci. Adv. 4 (2018) eaau0920.